JOURNAL OF GEOPHYSICAL RESEARCH, VOL. 113, B06404, doi:10.1029/2007JB005256, 2008

Effect of a compliant fault zone on the inferred earthquake slip distribution

Sylvain Barbot,[1] Yuri Fialko,[1] and Dave Sandwell[1]

Received 3 July 2007; revised 21 November 2007; accepted 27 December 2007; published 14 June 2008.

[1] We present a new semi-analytic method to evaluate the deformation due to a screw dislocation in arbitrarily heterogeneous and/or anisotropic elastic half plane. The method employs integral transformations to reduce the governing partial differential equations to the integral Fredholm equation of the second kind. Dislocation sources, as well as spatial perturbations in the elastic properties are modeled using equivalent body forces. The solution to the Fredholm equation is obtained in the Fourier domain using a method of successive over-relaxation, and is mapped into the spatial domain using the inverse Fast Fourier Transform. We apply this method to investigate the effect of a soft damage zone around an earthquake fault on the co-seismic displacement field, and on the earthquake slip distribution inferred from inversions of geodetic data. In the presence of a kilometer-wide damage zone with a reduction of the effective shear modulus of a factor of 2, inversions that assume a laterally homogeneous model tend to underestimate the amount of slip in the middle of the seismogenic layer by as much as 20%. This bias may accentuate the inferred maxima in the seismic moment release at depth between 3–6 km suggested by previous studies of large strike-slip earthquakes.

Citation: Barbot, S., Y. Fialko, and D. Sandwell (2008), Effect of a compliant fault zone on the inferred earthquake slip distribution, *J. Geophys. Res.*, *113*, B06404, doi:10.1029/2007JB005256.

1. Introduction

[2] Major crustal faults are often associated with zones of highly cracked and damaged rocks that can extend as far as 10^2–10^3 m away from the slip interface [*Ambraseys*, 1970a; *Wilson et al.*, 2004; *Chester et al.*, 2005]. Such zones may result from inelastic deformation associated with the fault growth [e.g., *Vermilye and Scholz*, 1998; *Manighetti et al.*, 2001] or repeated seismic ruptures [*Rice et al.*, 2005; *Fialko*, 2007]. Intense damage gives rise to a reduction in the effective elastic moduli of the fault zone material, as predicted by theoretical models [*Rybicki*, 1971; *Kachanov*, 1986; *Lyakhovsky et al.*, 2001; *Turcotte et al.*, 2003], and evidenced by geodetic [*Fialko et al.*, 2002; *Fialko*, 2004b; *Hamiel and Fialko*, 2007] and seismic [*Li et al.*, 1994; *Thurber et al.*, 2003; *Cochran et al.*, 2006] observations. Macroscopic compliant fault zones result in significant lateral variations in the mechanical properties of the Earth's crust, and may affect the pattern of surface deformation during the co-seismic, post-seismic, and inter-seismic phases of the earthquake cycle. In this paper we investigate the effect of a pre-existing damage zone on the co-seismic displacement field, and spatially variable fault slip inferred from inversions of geodetic data.

[3] We develop a new computationally efficient semi-analytic model of the fault-induced deformation in an arbitrarily heterogeneous and anisotropic medium. We use integral transforms to reduce the problem to the Fredholm integral equation of the second kind which is solved by means of successive approximations [e.g., *Delves and Mohamed*, 1985; *Fialko et al.*, 2001]. The forcing terms are the equivalent body forces representing dislocations with prescribed slip [*Eshelby*, 1957; *Burridge and Knopoff*, 1964]. Our approach takes advantage of the convolution theorem and the fast Fourier transforms [e.g., *Frigo and Johnson*, 1998] and avoids the formation of a stiffness matrix, such that the overall computational burden scales only linearly with the model size. The method readily allows one to simulate deformation due to fault slip in the Earth's crust or lithosphere with realistic variations in the elastic moduli (e.g., as inferred from seismic tomography data). It can be also extended to simulate the visco-elastic response by taking advantage of the correspondence principle, whereby the time-dependent response of a visco-elastic medium is determined by applying the Laplace transform and reducing a problem to a set of inhomogeneous static problems in the transformed domain [e.g., *Pollitz*, 1997; *Smith and Sandwell*, 2004; *Wang et al.*, 2006].

[4] In the next section, we present the elasto-static solution for heterogeneous media. The solution is implemented for a case of a two-dimensional anti-plane deformation, and verified against a number of available analytic solutions. In section 3, we apply our method to investigate the effects of

[1]Institute of Geophysics and Planetary Physics, Scripps Institution of Oceanography, University of California San Diego, La Jolla, California, USA.

0148-0227/08/2007JB005256$09.00

a macroscopic compliant fault zone on co-seismic slip distributions inferred from inversions of geodetic data.

2. Semi-Analytic Model of Deformation in Heterogeneous and Anisotropic Media

2.1. Theory

[5] Surface deformation due to slip on a fault can be well described using solutions for dislocations in an elastic half-space [*Steketee*, 1958; *Savage and Burford*, 1973; *Fialko*, 2004b]. As demonstrated by *Burridge and Knopoff* [1964], one may transform the corresponding mixed boundary-value problem into a stress boundary-value problem using a body-force equivalent of the dislocation discontinuity in terms of double couples. Under this approach, the solution can simply be obtained from the integration of some forcing terms $\mathbf{f}(\mathbf{x})$. The equivalent body force for a total displacement $\mathbf{u}$ on a fault located at position $\mathbf{x}$ and oriented normal to $\hat{\mathbf{n}}(\mathbf{x})$ (see Figure 1), in a linear elastic medium with an elasticity tensor $\mathbf{C}(\mathbf{x})$ is given by [e.g., *Eshelby*, 1957; *Burridge and Knopoff*, 1964; *Aki and Richards*, 1980; *Alshits and Kirchner*, 1995a, 1995b; *Nemat-Nasser and Hori*, 1999]

$$\mathbf{f} = -\nabla \cdot (\mathbf{C} : \mathbf{u} \otimes \hat{\mathbf{n}}) \tag{1}$$

The static deformation resulting from fault slip satisfies the conservation of linear momentum [e.g., *Malvern*, 1969]

$$\nabla \cdot \boldsymbol{\sigma} + \mathbf{f} = 0 \tag{2}$$

subjected to the displacement-strain relation $\boldsymbol{\epsilon} = \frac{1}{2}[\nabla \otimes \mathbf{u} + (\nabla \otimes \mathbf{u})^t]$, the stress-strain relation $\boldsymbol{\sigma} = \mathbf{C}$: $\boldsymbol{\epsilon}$, and appropriate boundary conditions. For a finite deformation source in an elastic half-space, the relevant boundary conditions are zero tractions at the free surface and vanishing displacements at infinity.

[6] We now introduce the following iterative approach to simulate a dislocation in a heterogeneous half-space. Consider the decomposition of the elastic moduli into a constant part $\bar{\mathbf{C}}$ and a heterogeneous part, $\mathbf{C}'(\mathbf{x})$ [e.g., *Du et al.*, 1994],

$$\mathbf{C}(\mathbf{x}) = \bar{\mathbf{C}} + \mathbf{C}'(\mathbf{x}) \tag{3}$$

The choice of $\bar{\mathbf{C}}$ is discussed in Appendix A. The conservation of linear momentum can then be written

$$\nabla \cdot (\bar{\mathbf{C}} : \boldsymbol{\epsilon}) + \mathbf{f} + \nabla \cdot (\mathbf{C}' : \boldsymbol{\epsilon}) = 0. \tag{4}$$

The contribution $\nabla \cdot (\mathbf{C}'$: $\boldsymbol{\epsilon})$ can be interpreted as equivalent body forces mimicking the presence of heterogeneities. These fictitious forces are uniquely related to the elastic structure and can be distributed such that the resulting deformation in a homogeneous medium is equivalent to that in a heterogeneous medium. The proposed algorithm for solving the heterogeneous problem consists in the following steps: first, starting from the displacement field $\mathbf{u}_0 = 0$ (or some non-trivial guess), compute the equivalent body force at iteration $n = 1$,

$$\tilde{\mathbf{f}}_n = \mathbf{f} + \nabla \cdot (\mathbf{C}' : \boldsymbol{\epsilon}_{n-1}), \tag{5}$$

then solve the homogeneous problem

$$\nabla \cdot (\bar{\mathbf{C}} : \boldsymbol{\epsilon}_n) + \tilde{\mathbf{f}}_n = 0 \tag{6}$$

for the entire displacement field with appropriate boundary conditions. Last, verify the convergence criterion

$$\frac{\left\langle \| \tilde{\mathbf{f}}_n - \tilde{\mathbf{f}}_{n-1} \|^2 \right\rangle}{\langle \| \mathbf{f} \|^2 \rangle} < \epsilon \tag{7}$$

where ϵ is the tolerance (hereafter, we use $\epsilon = 10^{-6}$), and the operator $\langle \, . \, \rangle$ denotes integration over the entire domain. Steps (5) and (6) are repeated until condition (7) is satisfied. The convergence criterion is a necessary condition to ensure that the equivalent body forces adequately mimic heterogeneities in the elastic structure. The amplitude of stress and the equivalent body forces is governed by the forcing term $\mathbf{f}$, which depends upon the magnitude of slip on the dislocations and the local shear modulus, so the convergence criterion (7) is scaled accordingly.

[7] The displacement field due to a dislocation in an arbitrarily heterogeneous material can be obtained by iteratively solving the corresponding homogeneous problems with the properly distributed body forces.

2.2. Anti-Plane Deformation

2.2.1. Implementation

[8] Here we implement the described procedure for the case of an infinitely long screw dislocation in an elastic half-space, with two-dimensional variations in shear modulus [e.g., *Barnett*, 1972; *Du et al.*, 1994]. The deformation is anti-plane strain, as $u_2 = u_3 = 0$, the only non-zero displacement component is $u_1 = u_1(x_2, x_3)$, and the only non-zero stress components are

$$\begin{aligned} \sigma_{12} &= 2\mu\,\epsilon_{12} = \mu\, u_{1,2} \\ \sigma_{13} &= 2\mu\,\epsilon_{13} = \mu\, u_{1,3} \end{aligned} \tag{8}$$

We now decompose the rigidity tensor into a constant part and a heterogeneous part as follows,

$$\mu(\mathbf{x}) = \bar{\mu} + \mu'(\mathbf{x}) \tag{9}$$

We use the method of images to satisfy the free-surface boundary condition [*Steketee*, 1958; *Smith and Sandwell*, 2004]. The equivalent body forces act in the x_1-direction only, and we write $f_1(\mathbf{x})$ the sum of the equivalent body forces and their image. The conservation of linear momentum can now be written as

$$\bar{\mu}\left(u_{1,22} + u_{1,33}\right) = -f_1 - \left(\mu' u_{1,2}\right)_{,2} - \left(\mu' u_{1,3}\right)_{,3} \tag{10}$$

which simplifies to the Poisson's equation in case of a homogeneous medium. After Fourier transforming, equation (10) is reduced to an algebraic expression representing the Fredholm integral equation of the second kind (see Appendix A).

[9] We solve equation (10) by using a method of successive approximations in the spectral domain. Convergence of the resulting series of iterated kernels is further discussed in

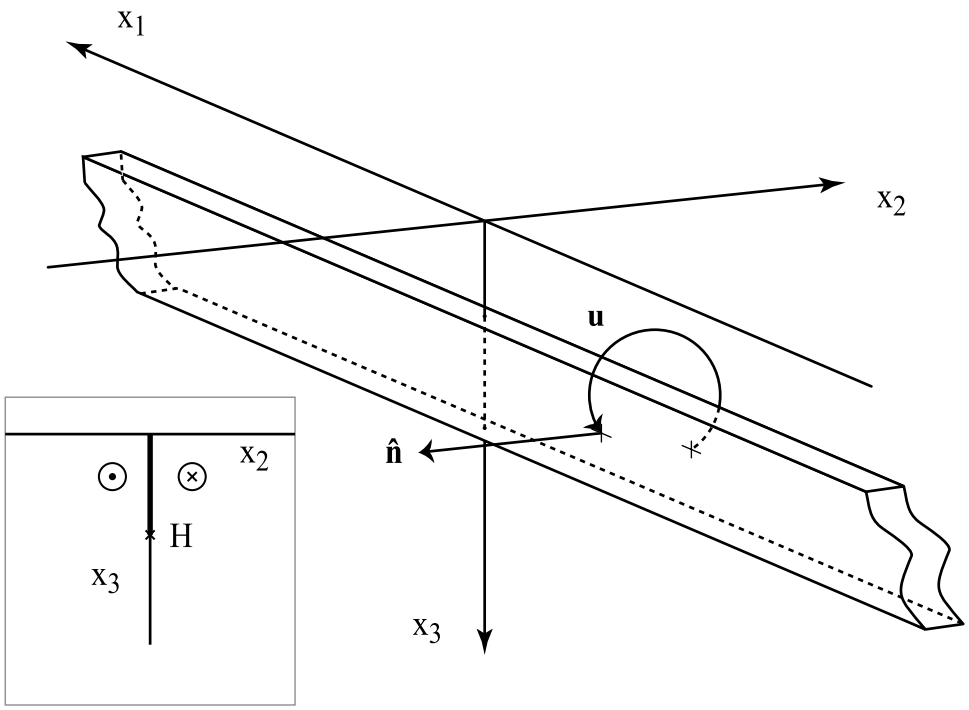

Figure 1. Dislocation in a half-space. A fault idealized by a plane of normal vector $\hat{\mathbf{n}}$ is sliding in a direction $\mathbf{u}$. In anti-plane deformation, strike-slip occurs along the x_1-direction.

the Appendix A. A similar approach was previously used to study the cooling of the oceanic lithosphere [*Sandwell*, 1984], the mantle convection [*Gable et al.*, 1991] and complex composites in mineral structures [*Moulinec and Suquet*, 1998; *Lebensohn*, 2001]. We employ the Successive Over-Relaxation (SOR) technique to accelerate convergence [e.g., *Golub and Van Loan*, 1996]. The iterative algorithm for solving equation (10) is as follows: Starting from $\hat{u}_1^0(\mathbf{k}) = 0$ or some initial guess, compute the equivalent body forces in the spectral domain for iteration $n = 1$

$$\begin{aligned}\hat{g}^n(\mathbf{k}) = \hat{f}_1 &- \omega_2\left(\hat{\mu}' * \omega_2\hat{u}_1^{n-1}\right)\\ &- \omega_3\left(\hat{\mu}' * \omega_3\hat{u}_1^{n-1}\right)\end{aligned} \tag{11}$$

where the hat denotes the relevant field in the transformed domain and we use $\boldsymbol{\omega} = 2\pi\mathbf{k}$. The two-dimensional convolutions, denoted by the symbol *, are performed in the space domain, taking advantage of the fast Fourier transform. Then, we update the displacement field using the SOR method

$$\hat{u}_1^n(\mathbf{k}) = \phi T(\mathbf{k})\hat{g}^n(\mathbf{k}) + (1-\phi)\hat{u}_1^{n-1}(\mathbf{k}) \tag{12}$$

where we have defined the transfer function

$$\hat{T}(\mathbf{k}) = \frac{1}{\bar{\mu}\left(\omega_2^2 + \omega_3^2\right)} \tag{13}$$

An optimal value for the SOR parameter ϕ for simple problems (single fault embedded in a subspace of uniform shear modulus) is $\phi = \bar{\mu}/\mu^*$ where μ^* is the shear modulus μ on the fault. This choice ensures the satisfaction of the boundary conditions on the fault at any iteration, so that the final solution is obtained with fewer iterations. If the geometry prohibits one from using this simple definition, the default value $\phi = 1$ should be preferred, which corresponds to the successive approximation approach. Finally, we evaluate the convergence criterion

$$\frac{\left\langle \| \hat{g}^n - \hat{g}^{n-1} \|^2 \right\rangle}{\left\langle \| \hat{f}_1 \|^2 \right\rangle} < \epsilon \tag{14}$$

where the norm is $\| f \|^2 = ff^*$, and the functional $\langle \|.\|^2 \rangle = \int_{-\infty}^{\infty} \|.\|^2 \, d\mathbf{k}$ denotes the total error inferred from the Rayleigh's theorem. In order to satisfy the boundary condition of vanishing of displacement at infinity, we need to enforce $\hat{u}_1^n(0) = 0$. This is done by setting $\hat{T}(0) = 0$. Steps (11) and (12) are to be repeated until the convergence test (14) is satisfied. The suggested algorithm uses the direct and inverse two-dimensional Fourier transforms

$$\begin{aligned}\hat{f}(\mathbf{k}) &= \int_{-\infty}^{\infty} f(\mathbf{x}) e^{-i2\pi\mathbf{k}\cdot\mathbf{x}} d\mathbf{x}\\ f(\mathbf{x}) &= \int_{-\infty}^{\infty} \hat{f}(\mathbf{k}) e^{i2\pi\mathbf{k}\cdot\mathbf{x}} d\mathbf{k}\end{aligned} \tag{15}$$

[10] The fault geometry is defined by the value of $f_1(\mathbf{x})$ and can be readily expressed in the Fourier domain in an analytic fashion. However, an accurate model depends upon the quality of the frequency sampling and the fault slip distribution should be tapered so that high frequencies vanish as one approaches the Nyquist frequency. We suggest two appropriate tapers which intensities are controlled by a roll-off parameter β. For any value of β in the range $0 < \beta < 1/2$, the tapers have a unit area and can be successively

added so that only the tip of the fault or abrupt changes in slip are tapered. The first is a linear taper

$$\Pi_\beta(x) = \begin{cases} 1, & |x| < \frac{1}{2} - \beta \\ \frac{1}{2\beta}\left(\frac{1}{2} + \beta - |x|\right), & \frac{1}{2} - \beta < |x| < \frac{1}{2} + \beta \\ 0, & \text{otherwise} \end{cases} \quad (16)$$

$$\tilde{\Pi}_\beta(k) = \text{sinc}(k)\text{sinc}(2\beta k)$$

The second taper suppresses stress singularities at the tip of a fault and allows for a better frequency sampling,

$$\Omega_\beta(x) = \begin{cases} 1, & |x| < \frac{1-2\beta}{2(1-\beta)} \\ \cos\left(\pi \frac{(1-\beta)|x| - \frac{1}{2} + \beta}{2\beta}\right)^2, & \frac{1-2\beta}{2(1-\beta)} < |x| < \frac{1}{2(1-\beta)} \\ 0, & \text{otherwise} \end{cases} \quad (17)$$

$$\tilde{\Omega}_\beta(k) = \frac{\text{sinc}\left(\frac{k}{1-\beta}\right) + (1-2\beta)\text{sinc}\left(k\frac{1-2\beta}{1-\beta}\right)}{2\left(1 - \beta - 4k^2\frac{\beta^2}{1-\beta}\right)}$$

For $\beta = 0$, both tapers reduce to a simple boxcar function. As an example, a vertical fault of unit length and slip, starting at depth d, has the equivalent body-force in the Fourier domain

$$\hat{f}_1(\mathbf{k}) = -\mu * i2\pi k_2 e^{-\pi^2 \Delta x_2^2 k_2^2} \times \tilde{\Omega}_\beta(k_3) 2\cos(2\pi k_3(1/2 + d)) \quad (18)$$

where we make use of the Gaussian representation of a unit moment, Δx_2 being the horizontal sampling interval, and we utilize the shift property of the Fourier transform to add the source and its image.

2.2.2. Benchmarks

[11] We test our semi-analytic solution against a number of available analytic solutions for an elastic half-space with the spatially variable elastic moduli. All benchmarks discussed below include a strike-slip fault extending from the surface to a depth L, and having the surface slip s. Our method allows one to treat dipping faults; for simplicity, here we restrict our attention to vertical faults only.

[12] We begin with the case of an isotropic medium with a contrast in shear modulus across a transform fault (Figure 2a). The analytic solution for the surface displacement is

$$u_1(x_2) = \begin{cases} \frac{2s}{\pi}\frac{\mu_2}{\mu_1 + \mu_2}\tan^{-1}\frac{L}{x_2}, & x_2 < 0 \\ \frac{2s}{\pi}\frac{\mu_1}{\mu_1 + \mu_2}\tan^{-1}\frac{L}{x_2}, & x_2 > 0 \end{cases} \quad (19)$$

where μ_1 and μ_2 are the value of the shear modulus at each side of the fault and s is the total slip across the dislocation. As expected, the deformation is enhanced in the softer region. Note an excellent agreement between the numerical and analytic solutions.

[13] Next example illustrates the full post-seismic relaxation due to a visco-elastic substrate underlying the elastic-brittle layer (Figure 2b). Viscous flow reduces the co-seismically induced shear stresses below the brittle-ductile transition. In the limit of full relaxation and no secular deformation, the latter effectively becomes a stress-free boundary [e.g., *Fialko*, 2004c]. The full visco-elastic deformation can be evaluated by subtracting the elastic half-space and the elastic plate solutions. The respective analytic solutions are available for the case of the anti-plane strain [*Weertman and Weertman*, 1964; *Rybicki*, 1971; *Nur and Mavko*, 1974; *Barbot et al.*, 2008]. Because of the finite displacement at far field, a numerical cosine transform is more adequate to model the deformation. Our numerical solution is in an excellent agreement with the analytic expressions (see Figure 2). Note that the use of the SOR method allows one to treat such problems with arbitrarily large variations in elastic properties, as shown in this example.

[14] We now consider deformation due to slip on a fault embedded in a relatively narrow zone of damaged material having a reduced effective shear modulus. An analytic solution is available in the form of an infinite series [e.g., *Rybicki and Kasahara*, 1977]. The corresponding surface deformation is shown in Figure 2. The semi-analytic solution well captures the localized deformation including a discontinuity in strain at the interface between the fault zone and the surrounding crust. The convergence is reached after 2 iterations, which takes only a few seconds for a 512×512 array on a low end laptop computer.

[15] Finally, we consider the case of faulting in an anisotropic half plane with heterogeneous shear moduli. The condition of anti-plane strain requires that the dislocation lines extend along an axis of two-fold symmetry in the elastic moduli tensor. A fault separating two media with anisotropic shear moduli μ_{12} and μ_{13} satisfies this condition. Any anti-plane isotropic solution can be generalized for the anisotropic case by scaling the horizontal coordinate by a factor

$$\alpha = \sqrt{\frac{\mu_{13}}{\mu_{12}}} \quad (20)$$

Deformation in the presence of anisotropic heterogeneity across a transform fault, as sketched in Figure 2d, exhibits the following deformation profile at the surface:

$$u_1(x_2) = \begin{cases} \frac{2s}{\pi}\frac{1}{1+\alpha}\tan^{-1}\frac{L}{\alpha x_2}, & x_2 < 0 \\ \frac{2s}{\pi}\frac{\alpha}{1+\alpha}\tan^{-1}\frac{L}{x_2}, & x_2 > 0. \end{cases} \quad (21)$$

and is very well matched by the numerical solution (Figure 2d). The wavelength of the deformation is larger on the left side of the fault where the medium is more compliant in the vertical direction. Solutions for dislocations in heterogeneous anisotropic media are further discussed in Appendix B.

[16] As one can see from Figure 2, there is a general agreement between our semi-analytic approach and closed form analytic solutions. We conclude that the proposed iterative scheme can be efficiently used to model crustal

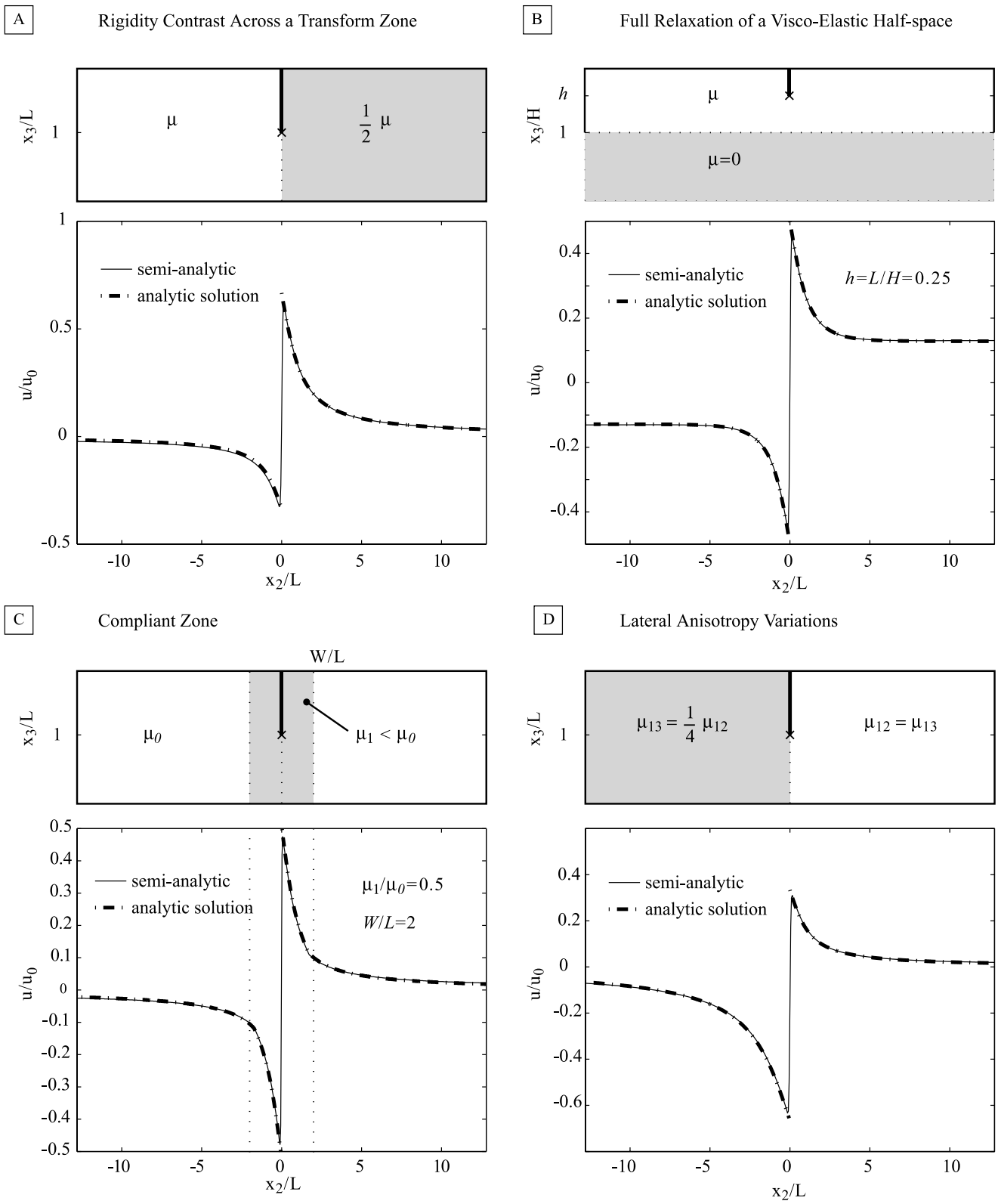

Figure 2. Comparison between the analytic expressions and the numerical solutions for surface displacements due to a fault slip in heterogenous media. a) Isotropic medium with a contrast of shear modulus across the transform fault zone. b) Isotropic medium after full relaxation of a visco-elastic substrate below the depth H. c) Isotropic medium with the compliant fault zone with total width $2W$. d) Contrast of anisotropy across the fault plane. The wavelength of deformation is larger in the softer anisotropic crust, to the left of the rupture.

deformation in the presence of arbitrary variations in the effective elastic moduli in the Earth's crust.

3. Co-Seismic Deformation in the Presence of a Compliant Fault Zone

[17] Major crustal faults are often surrounded by zones of highly cracked and damaged rocks, as evidenced by geologic [e.g., *Wilson et al.*, 2004; *Chester et al.*, 2005; *Dor et al.*, 2006], seismic [*Li et al.*, 1994; *Thurber et al.*, 2003; *Cochran et al.*, 2006] and geodetic [*Fialko et al.*, 2002; *Fialko*, 2004b; *Hamiel and Fialko*, 2007] observations. Such zones introduce significant lateral variations in the crustal rigidity, and likely affect patterns of co-seismic deformation at the Earth's surface (see Figure 2c). Consequently, inversions of geodetic data for the subsurface fault slip that are usually based on solutions for homogeneous or horizontally stratified Earth's crust may be systematically biased.

[18] We investigate this potential bias by modeling the co-seismic response of a heterogeneous brittle-elastic lithosphere in the presence of a damaged compliant fault zone. We approximate the damage zone by using a reduced shear modulus μ in a finite vertical strip centered on the fault plane and extending by the distance W in both directions away from the fault plane. On the basis of preliminary results from seismic tomography of the Calico fault zone in eastern California [*Cochran et al.*, 2006], we assume that the effective shear modulus varies gradually from a background value μ to a minimum value $\mu/2$ at the center of the fault zone. We further assume that the fault zone width is six times smaller than the depth extent of the co-seismic slip, $W = L/6$, where L is the nominal locking depth. For a fault locking depth of 12 km typical of California, the assumed thickness of the compliant zone is 2 km, consistent with some geodetic and seismic observations [*Fialko et al.*, 2002; *Fialko*, 2004b; *Hamiel and Fialko*, 2007; *Cochran et al.*, 2006]. The fault slip is assumed to be constant in the uppermost crust, and gradually tapered to zero toward the bottom of the seismogenic zone according to the following expression,

$$s(x_3) = s_0\left(\Pi_\beta\left[\frac{2x_3 - L}{2L}\right] + \Pi_\beta\left[\frac{2x_3 + L}{2L}\right]\right) \qquad (22)$$

where s_0 is slip in the upper part of the fault. The assumed slip distribution is shown by the solid line in Figure 3b for $\beta = 0.4$. The corresponding surface displacements are shown in Figure 3a for a homogeneous half-space (solid line) and a half-space with the compliant fault zone (dashed line). The difference between the two model predictions is maximum at a distance of $O(W)$ away from the fault, where it reaches $\sim$10% of the local displacement amplitude.

[19] We then invert the synthetic co-seismic surface displacements for the fault slip distribution at depth. Using the Green's functions for a homogeneous elastic half-space, we perform two sets of inversions: one for the case of a heterogeneous half-space with a compliant zone, and another for the case of a homogeneous elastic half-space. The corresponding surface displacements are shown in Figure 3a. As inversions of surface displacements are intrinsically non-unique [e.g., *Parker*, 1994a; *Mavko*, 1981; *Savage*, 1990], we impose the non-negativity and smoothness constraints to regularize the problem [see *Fialko*, 2004b]. The resulting slip distributions are shown in Figure 3b for the homogeneous (long dashed line) and heterogeneous (short dashed line) models. Note that the use of the non-negativity constraint makes the inversion a non-linear one. One consequence of non-linearity is that the difference between the inverted slip models (e.g., corresponding to the homogeneous and heterogeneous forward models) is not equivalent to the inversion of the difference between the surface displacements (Figure 3a). Figures 3c and 3d illustrate results of the inversion of the difference between the synthetics for the homogeneous and heterogeneous half-space, and the difference between the slip distributions shown in Figure 3b, respectively. A comparison between the slip models inferred from inversions, and the assumed slip distribution (Figure 3b) shows that the neglect of a compliant fault zone gives rise to an underestimation of slip throughout much of the seismogenic layer. The largest discrepancy (as much as 20%) corresponds to a depth interval around $x_3 \sim 0.2\ L$. In addition, inversions neglecting a compliant zone tend to overestimate slip below the effective brittle-ductile transition (depths greater than L, see Figure 3b). The effect of a vertical compliant zone on the inferred slip distribution is opposite to the effect of horizontal layering. The latter tends to bias the moment centroid to shallower depths in slip inversions that assume a homogeneous elastic half-space [*Simons et al.*, 2002; *Fialko*, 2004a; *Hearn and Bürgmann*, 2005].

[20] These results bear on the interpretation of co-seismic deformation. In particular, inversions of high-quality geodetic data from several large strike-slip events including the Landers, Izmit, Hector Mine, and Bam earthquakes [*Simons et al.*, 2002; *Fialko*, 2004b; *Fialko et al.*, 2005] suggest that the maximum seismic moment release occurs in the middle of the seismogenic layer, with a peak in the interval between 3 and 6 km [*Fialko et al.*, 2005]. Because co-seismic slip in the uppermost part of the brittle layer (shallower than $\sim$3 km) appears to be systematically less than slip at greater depth, this pattern was referred to as the "shallow slip deficit" [*Simons et al.*, 2002; *Fialko et al.*, 2005]. It is of interest to establish whether the shallow slip deficit inferred from inversions of geodetic data represents actual variations in seismic slip with depth, or is an artifact of inversions (e.g., due to an oversimplified representation of the mechanical response of the Earth's crust to fault slip). Results presented above suggest that previous inferences of the shallow slip deficit may be in fact conservative, as inversions based on homogeneous or horizontally stratified elastic half-space models likely underestimate the amount of slip in the depth interval between $\sim$3–6 km if earthquake faults are embedded in large damage zones with reduced effective elastic moduli (Figure 3b).

[21] The semi-analytic approach described in this paper allows one to accurately and efficiently calculate deformation due to fault slip in a heterogeneous elastic half-space under conditions of anti-plane strain. This approach can be readily extended for the general case of three-dimensional (3-D) deformation. The 3-D formulation will be presented in a separate paper.

4. Conclusions

[22] We derived an iterative approach to model dislocations in heterogeneous and anisotropic media for the case of

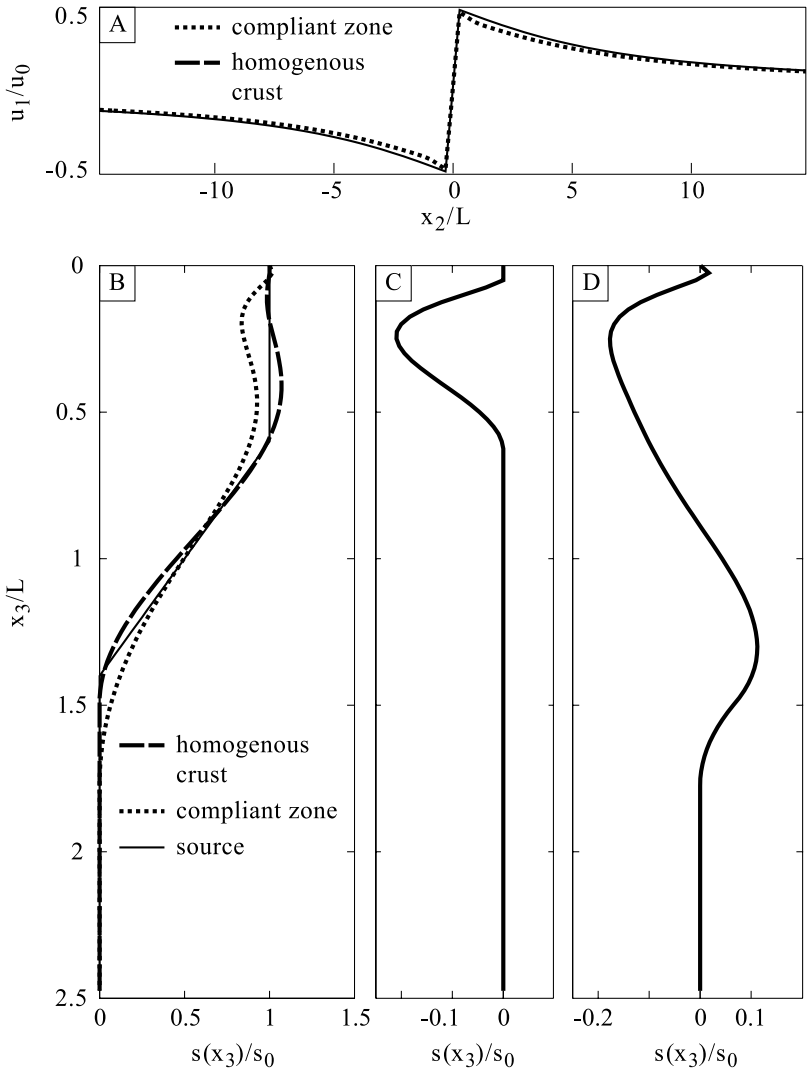

Figure 3. (a) Synthetic co-seismic surface displacements in a homogeneous crust (solid line) and in a laterally heterogeneous crust with a compliant zone (dashed line). (b) Slip inversions of surface displacements for the initial slip distribution shown by the continuous profile. (c) Inversion of the algebraic difference between the homogeneous and the heterogeneous synthetics. (d) Difference between the inversions of the homogeneous and heterogeneous synthetics.

two-dimensional (anti-plane strain) deformation appropriate for infinitely long strike-slip faults. The method requires solving homogeneous problems with equivalent body forces that account for arbitrarily distributed elastic heterogeneities in the Earth's crust. By making use of a series of integral transforms, the problem is reduced to the Fredholm integral equation of the second kind. The computational burden is alleviated by the application of the convolution theorem and the use of fast Fourier transforms. We have tested our numerical scheme against analytic solutions for surface displacements due to a finite dislocation with variable slip. The comparisons showed a very good agreement between the numerical and analytic solutions, indicating that the proposed method can be used to model deformation in heterogeneous and anisotropic media with essentially arbitrary distribution of elastic moduli.

[23] We applied the Fredholm iterative scheme to model the co-seismic displacements in the presence of a narrow compliant zone with gradual variations in the shear modulus. Inversions of the corresponding surface displacements for subsurface fault slip show that models that neglect the presence of compliant damage zones around earthquake faults may underestimate fault slip by as much as 20% in the middle of the seismogenic layer. This bias implies more accentuated shallow slip deficit than suggested by previous studies of large strike-slip earthquakes, provided that the investigated earthquake ruptures are surrounded by wide damage zones.

Appendix A: Convergence Condition

[24] The displacement field due to a screw dislocation in a heterogeneous isotropic medium is, when expressed in the

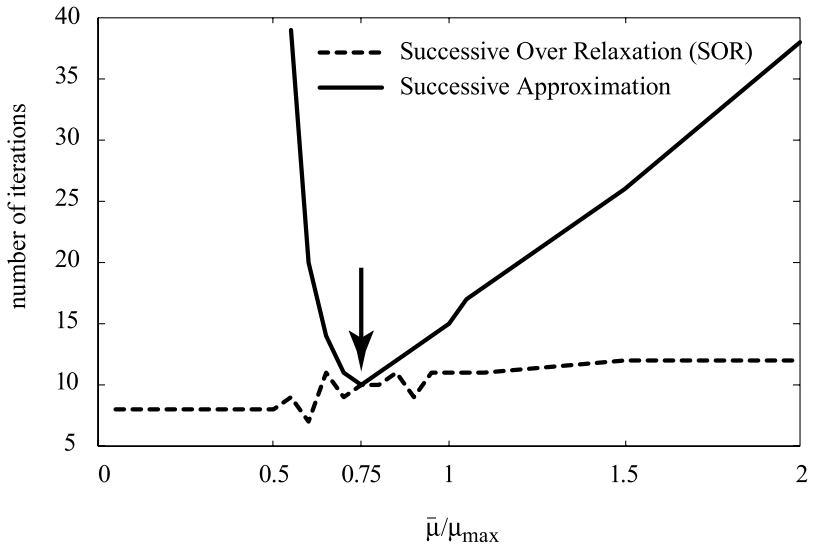

Figure A1. Convergence rate of the proposed algorithm as a function of the homogenization constant $\bar{\mu}$. The successive approximation works best for the value predicted by equation (A11) (as denoted by arrow). When using SOR, convergence is obtained for all range of $\bar{\mu}$ with an accelerated rate.

Fourier domain, the solution of the Fredholm integral of the second kind

$$\hat{u}(\mathbf{k}) = \frac{\hat{f}_2}{\bar{\mu}\, 4\pi^2 \mathbf{k}\cdot\mathbf{k}} + \int_{-\infty}^{\infty} K(\mathbf{k},\mathbf{s})\hat{u}(\mathbf{s})d\mathbf{s} \tag{A1}$$

where the kernel $K(\mathbf{k}, \mathbf{s})$ is

$$K(\mathbf{k},\mathbf{s}) = \frac{\mathbf{k}\cdot\mathbf{s}}{\mathbf{k}\cdot\mathbf{k}}\frac{\hat{\mu}'(\mathbf{k}-\mathbf{s})}{\bar{\mu}}. \tag{A2}$$

The estimation of $\hat{u}(\mathbf{k})$ can be performed by successive approximations

$$\hat{u}(\mathbf{k})^n = T\left[\hat{u}(\mathbf{k})^{n-1}\right]. \tag{A3}$$

The corresponding series converges if

$$\|T[\hat{u}(\mathbf{k})^n] - T[\hat{u}(\mathbf{k})^{n+1}]\| < \|\hat{u}(\mathbf{k})^n - \hat{u}(\mathbf{k})^{n+1}\| \tag{A4}$$

where we use the infinite norm

$$\|f\|^2 = \max_{\mathbb{R}^2} f(\mathbf{k}) f^*(\mathbf{k}) \tag{A5}$$

As T[.] is a linear operator, we can write

$$\begin{aligned} T\left[\hat{u}^n\right] - T\left[\hat{u}^{n+1}\right] &= T\left[\hat{u}^n - \hat{u}^{n+1}\right] \\ &= \int_{-\infty}^{\infty} K(\mathbf{k},\mathbf{s})\left(\hat{u}(\mathbf{s})^n - \hat{u}(\mathbf{s})^{n+1}\right)d\mathbf{s} \end{aligned} \tag{A6}$$

Applying the Cauchy-Schwarz inequality, we have

$$\begin{aligned} &\left\| \int_{-\infty}^{\infty} K(\mathbf{k},\mathbf{s})\left(\hat{u}(\mathbf{s})^n - \hat{u}(\mathbf{s})^{n+1}\right)d\mathbf{s} \right\| \\ &\quad < \left\| \int_{-\infty}^{\infty} K(\mathbf{k},\mathbf{s})d\mathbf{s} \right\| \left\| \hat{u}(\mathbf{k})^n - \hat{u}(\mathbf{k})^{n+1} \right\| \end{aligned} \tag{A7}$$

Combining equations (A4) and (A7), the convergence of the successive approximation method is obtained if

$$\left\| \int_{-\infty}^{\infty} K(\mathbf{k},\mathbf{s})d\mathbf{s} \right\| < 1 \tag{A8}$$

Evaluation of the above integral gives

$$\begin{aligned} \int_{-\infty}^{\infty} K(\mathbf{k},\mathbf{s})d\mathbf{s} &= \int_{-\infty}^{\infty} \frac{\mathbf{k}\cdot\mathbf{s}}{\mathbf{k}\cdot\mathbf{k}}\frac{\hat{\mu}'(\mathbf{k}-\mathbf{s})}{\bar{\mu}}d\mathbf{s} \\ &= \int_{-\infty}^{\infty} \frac{\hat{\mu}'(\mathbf{s})}{\bar{\mu}}d\mathbf{s} - \int_{-\infty}^{\infty} \frac{\mathbf{k}\cdot\mathbf{s}}{\mathbf{k}\cdot\mathbf{k}}\frac{\hat{\mu}'(\mathbf{s})}{\bar{\mu}}d\mathbf{s} \\ &= \frac{\mu'(0)}{\bar{\mu}} + \frac{i2\pi\mathbf{k}\cdot\nabla\mu'(0)}{-4\pi^2\mathbf{k}\cdot\mathbf{k}\,\bar{\mu}} \end{aligned} \tag{A9}$$

where the last step is obtained by application of the moment theorem [*Bracewell*, 2003]. We also require invariant convergence properties upon translation, so after Fourier transforming (A9) to the space domain, one obtains the convergence criterion

$$\left|\frac{\mu'(\mathbf{x})}{\bar{\mu}}\right| < \frac{1}{2} \tag{A10}$$

where $|.|$ denotes the absolute value. The optimal choice for $\bar{\mu}$, that allows the maximum range of deviations, is

$$\bar{\mu} = \frac{1}{2}\left(\max_{\mathbb{R}^2}\mu(\mathbf{x}) + \min_{\mathbb{R}^2}\mu(\mathbf{x})\right) \tag{A11}$$

[25] We have implemented the suggested algorithm for the case of the transform fault (Figure 2a) and performed a series of calculations for various values of $\bar{\mu}$. Results shown in Figure A1 indicate that convergence is obtained only for $\bar{\mu}$ min $\mu(\mathbf{x})$ and that the optimal convergence rate is obtained for the value predicted by (A11). When using

SOR, there is much less sensitivity to the choice of $\bar{\mu}$, as convergence is always reached, and convergence rates are always faster compared to the successive approximation method.

Appendix B: Anisotropy

[26] Here we implement the suggested procedure for the case of anti-plane strain in the presence of arbitrary heterogeneity and anisotropy. The non-zero stress components are

$$\begin{aligned}\sigma_{12} &= 2C_{1212}\varepsilon_{12} = \mu_{12}u_{1,2}\\ \sigma_{13} &= 2C_{1313}\varepsilon_{13} = \mu_{13}u_{1,3}\end{aligned} \tag{B1}$$

where we denote, for the sake of simplicity, the shear moduli as $\mu_{12} = C_{1212}$ and $\mu_{13} = C_{1313}$. Note that for an isotropic medium, $\mu = C_{1212} = C_{1313}$. The rigidity tensor is decomposed into a constant part and a heterogeneous part as follows,

$$\begin{aligned}\mu_{12}(\mathbf{x}) &= \bar{\mu}_{12} + \mu'_{12}(\mathbf{x})\\ \mu_{13}(\mathbf{x}) &= \bar{\mu}_{13} + \mu'_{13}(\mathbf{x})\end{aligned} \tag{B2}$$

and the conservation of linear momentum is written

$$\bar{\mu}_{12}u_{1,22} + \bar{\mu}_{13}u_{1,33} = -f_1 - \left(\mu'_{12}u_{1,2}\right)_{,2} - \left(\mu'_{13}u_{1,3}\right)_{,3} \tag{B3}$$

The algorithm is essentially the same as in the isotropic case, but the equivalent body forces, corresponding to (11) in the isotropic case, become

$$\hat{g}^n(\mathbf{k}) = \hat{f}_1 - \omega_2\left(\hat{\mu}'_{12} * \omega_2\hat{u}_1^{n-1}\right) - \omega_3\left(\hat{\mu}'_{13} * \omega_3\hat{u}_1^{n-1}\right) \tag{B4}$$

The transfer function is

$$\hat{T}(\mathbf{k}) = \left(\bar{\mu}_{12}\omega_2^2 + \bar{\mu}_{13}\omega_3^2\right)^{-1} \tag{B5}$$

and an optimal value for the SOR parameter is now $\phi = \bar{\mu}_{12}/\mu^*_{12}$ where μ^*_{12} is the horizontal shear modulus μ_{12} on the fault. Similarly, the relevant elastic parameter for the body force representation in the presence of anisotropy is μ_{12} [*Burridge and Knopoff*, 1964]. As an example, a vertical fault of length L and slip s, starting at depth d, has the equivalent body-force

$$\begin{aligned}\hat{f}_1(\mathbf{k}) = &- s\mu^*_{12}i2\pi k_2 e^{-\pi^2\Delta x_2^2 k_2^2}\\ &\times L\,\tilde{\Omega}_\beta(L\,k_3)2\cos(2\pi k_3(L/2+d))\end{aligned} \tag{B6}$$

Our solution for a dislocation in a heterogeneous and anisotropic half plane favorably compares to the analytic one, as shown in Figure 2 in the main text.

[27] **Acknowledgments.** We thank Associate Editor Johannes Weertman and two anonymous reviewers for their thorough and thoughtful reviews of this manuscript. We thank Glenn Ierley for sharing his insight on numerical methods and in particular for suggesting the use of the SOR approach. This work was supported by NSF (grant EAR-0450035) and SCEC. Numerical codes used in this study are available from the authors.

References

Aki, K., and P. G. Richards (1980), *Quantitative Seismology*, vol. I, W. H. Freeman and Company, New York.

Alshits, V. I., and H. O. K. Kirchner (1995a), Elasticity of multilayers. I. Basic equations and solutions, *Philos. Mag. A and B*, *72*, 1431–1444.

Alshits, V. I., and H. O. K. Kirchner (1995b), Elasticity of multilayers. II. Strips, coatings and sandwiches, *Philos. Mag. A and B*, *72*, 1445–1470.

Ambraseys, N. (1970), Some characteristic features of the North Anatolian fault zone, *Tectonophysics*, *9*, 143–165.

Barbot, S., Y. Hamiel, and Y. Fialko (2008), Space geodetic investigation of the coseismic and postseismic deformation due to the 2003 M_w 7.2 Altai earthquake: Implications for the local lithospheric rheology, *J. Geophys. Res.*, *113*, B03403, doi:10.1029/2007JB005063.

Barnett, D. M. (1972), On the screw dislocation in an inhomogeneous elastic medium: The case of continuously varying elastic moduli, *Int. J. Solids Struct.*, *8*, 651–660.

Bracewell, R. (2003), The Fourier transform and its applications, in *Electrical and Computer Engineering*, 3rd ed., Tata McGraw-Hill, New York.

Burridge, R., and L. Knopoff (1964), Body force equivalents for seismic dislocations, *Bull. Seismol. Soc. Am.*, *54*, 1875–1888.

Chester, J. S., F. M. Chester, and A. K. Kronenberg (2005), Fracture surface energy of the Punchbowl fault, San Andreas system, *Nature*, *437*, 133–136.

Cochran, E. S., M. Radiguet, P. M. Shearer, Y.-G. Li, Y. Fialko, and J. E. Vidale (2006), Seismic imaging of the damage zone around the Calico fault, *Eos Trans. AGU*, *87*(52), Suppl., abst. T23E-03.

Delves, L., and J. Mohamed (1985), *Computational Methods for Integral Equations*, 373 pp., Cambridge Univ. Press, New York.

Dor, O., Y. Ben-Zion, J. Rockwell, and T. K. Brune (2006), Pulverized rocks in the Mojave section of the San Andreas fault zone, *Earth Planet. Sci. Lett.*, *245*, 642–654.

Du, Y., P. Segall, and H. Gao (1994), Dislocations in inhomogeneous media via a moduli perturbation approach: General formulation and two-dimensional solutions, *J. Geophys. Res.*, *99*(B7), 13,767–13,779.

Eshelby, J. D. (1957), The determination of the elastic field of an ellipsoidal inclusion, and related problems, *Proc. R. Soc., Ser. A and Ser. B*, *241*, 376–396.

Fialko, Y. (2004a), Probing the mechanical properties of seismically active crust with space geodesy: Study of the co-seismic deformation due to the 1992 M_w7.3 Landers (southern California) earthquake, *J. Geophys. Res.*, *109*, B03307, doi:10.1029/2003JB002756.

Fialko, Y. (2004b), Probing the mechanical properties of seismically active crust with space geodesy - Study of the coseismic deformation due to the 1992 Mw 7.3 Landers (Southern California) earthquake, *J. Geophys. Res.*, *109*, B03307, doi:10.1029/2003JB002756.

Fialko, Y. (2004c), Evidence of fluid-filled upper crust from observations of postseismic deformation due to the 1992 m_w 7.3 Landers earthquake, *J. Geophys. Res.*, *109*, B08401, doi:10.1029/2004JB002985.

Fialko, Y. (2007), Fracture and frictional mechanics - Theory, in *Treatise on Geophysics*, vol. 4, edited by G. Schubert, pp. 83–106, Elsevier Ltd., Oxford.

Fialko, Y., Y. Khazan, and M. Simons (2001), Deformation due to a pressurized horizontal circular crack in an elastic half-space, with applications to volcano geodesy, *Geophys. J. Int.*, *146*, 181–190.

Fialko, Y., D. Sandwell, D. Agnew, M. Simons, P. Shearer, and B. Minster (2002), Deformation on nearby faults induced by the 1999 hector mine earthquake, *Science*, *297*, 1858–1862.

Fialko, Y., D. Sandwell, M. Simons, and P. Rosen (2005), Three-dimensional deformation caused by the Bam, Iran, earthquake and the origin of shallow slip deficit, *Nature*, *435*, 295–299.

Frigo, M., and S. G. Johnson (1998), FFTW: An adaptative software architecture for the FFT, in *ICASSP Conference Proceedings*, vol. 3, pp. 1381–1384.

Gable, C. W., R. J. O'Connell, and B. J. Travis (1991), Convection in three dimensions with surface plates: Generation of toroidal flow, *J. Geophys. Res.*, *96*(B5), 8391–8405.

Golub, G. H., and C. F. Van Loan (1996), Iterative methods for linear systems, in *Matrix Computations*, 3rd ed., Johns Hopkins U. Press, Baltimore, MD.

Hamiel, Y., and Y. Fialko (2007), Structure and mechanical properties of faults in the North Anatolian fault system from InSAR observations of coseismic deformation due to the 1999 Izmit (Turkey) earthquake, *J. Geophys. Res.*, *112*, B07412, doi:10.1029/2006JB004777.

Hearn, E., and R. Bürgmann (2005), The effect of elastic layering on inversions of GPS data for coseismic slip and resulting stress changes: Strike-slip earthquakes, *Bull. Seismol. Soc. Am.*, *95*, 1637–1653.

Kachanov, L. (1986), *Introduction to Continuum Damage Mechanics*, Martinus Nijhoff, Dordrecht.

Lebensohn, R. A. (2001), N-site modelling of a 3D viscoplastic polycrystal using the fast Fourier transform, *Acta Mater.*, *49*, 2723–2737.

Li, Y., J. Vidale, K. Aki, C. Marone, and W. Lee (1994), Fine-structure of the Landers fault zone - Segmentation and the rupture process, *Science*, *265*, 367–370.

Lyakhovsky, V., Y. Ben-Zion, and A. Agnon (2001), Earthquake cycle, fault zones, and seismicity patterns in a rheologically layered lithosphere, *J. Geophys. Res.*, *106*(B3), 4103–4120.

Malvern, L. E. (1969), *Introduction to the Mechanics of a Continuum Medium*, 713 pp., Prentice-Hall, Englewood Cliffs, NJ.

Manighetti, I., G. King, Y. Gaudemer, C. Scholz, and C. Doubre (2001), Slip accumulation and lateral propagation of active normal faults in Afar, *J. Geophys. Res.*, *106*(B7), 13,667–13,696.

Mavko, G. M. (1981), Mechanics of motion on major faults, *Ann. Rev. Earth Planet. Sci.*, *9*, 81–111.

Moulinec, H., and P. Suquet (1998), A numerical method for computing the overall response of nonlinear composites with complex microstructure, *Comput. Methods Appl. Mech. Eng.*, *157*, 69–94.

Nemat-Nasser, S., and M. Hori (1999), *Micromechanics: Overall Properties of Heterogeneous Materials*, 2nd ed., Elsevier.

Nur, A., and G. Mavko (1974), Postseismic viscoelastic rebound, *Science*, *183*, 204–206.

Parker, R. L. (1994), *Geophysical Inverse Theory*, Princeton University Press, Princeton, NJ.

Pollitz, F. F. (1997), Gravitational viscoelastic postseismic relaxation on a layered spherical Earth, *J. Geophys. Res.*, *102*(B8), 17,921–17,941.

Rice, J. R., C. G. Sammis, and R. Parsons (2005), Off-fault secondary failure induced by a dynamic slip pulse, *Bull. Seismol. Soc. Am.*, *95*, 109–134.

Rybicki, K. (1971), The elastic residual field of a very long strike-slip fault in the presence of a discontinuity, *Bull. Seismol. Soc. Am.*, *61*, 79–92.

Rybicki, K., and K. Kasahara (1977), A strike-slip fault in a laterally inhomogeneous medium, *Tectonophysics*, *42*, 127–138.

Sandwell, D. T. (1984), Thermomechanical evolution of oceanic fracture zones, *J. Geophys. Res.*, *89*(B13), 11,401–11,413.

Savage, J. C. (1990), Equivalent strike-slip earthquakes cycles in half-space and lithosphere-asthenosphere earth models, *J. Geophys. Res.*, *95*(B4), 4873–4879.

Savage, J., and R. Burford (1973), Geodetic determination of relative plate motion in central California, *J. Geophys. Res.*, *78*(5), 832–845.

Simons, M., Y. Fialko, and L. Rivera (2002), Coseismic deformation from the 1999 M_w7.1 Hector Mine, California, earthquake, as inferred from InSAR and GPS observations, *Bull. Seismol. Soc. Am.*, *92*, 1390–1402.

Smith, B., and D. Sandwell (2004), A three-dimensional semianalytic viscoelastic model for time-dependent analyses of the earthquake cycle, *J. Geophys. Res.*, 109, B12401, doi:10.1029/2004JB003185.

Steketee, J. A. (1958), Some geophysical applications of the elasticity theory of dislocations, *Can. J. Phys.*, *36*, 1168–1198.

Thurber, C., S. Roecker, K. Roberts, M. Gold, L. Powell, and K. Rittger (2003), Earthquake locations and three-dimensional fault zone structure along the creeping section of the San Andreas fault near Parkfield, CA: Preparing for SAFOD, *Geophys. Res. Lett.*, *30*(3), 1112, doi:10.1029/2002GL016004.

Turcotte, D., W. Newman, and R. Shcherbakov (2003), Micro and macroscopic models of rock fracture, *Geophys. J. Int.*, *152*, 718–728.

Vermilye, J., and C. Scholz (1998), The process zone: A microstructural view of fault growth, *J. Geophys. Res.*, *103*(B6), 12,223–12,237.

Wang, R., F. Lorenzo-Martin, and F. Roth (2006), PSGRN/PSCMP-A new code for calculating co- and post-seismic deformation, geoid and gravity changes based on the viscoelastic-gravitational dislocation theory, *Comput. Geosci.*, *32*, 527–541.

Weertman, J., and J. R. Weertman (1964), *Elementary Dislocation Theory*, Macmillan, New York.

Wilson, B., T. Dewers, Z. Reches, and J. Brune (2004), Particle size and energetics of gouge from earthquake rupture zones, *Nature*, *434*, 749–752.

S. Barbot, Y. Fialko, and D. Sandwell, Institute of Geophysics and Planetary Physics, Scripps Institution of Oceanography, University of California San Diego, 9500 Gilman Drive, La Jolla, CA 92093-0225, USA. (sbarbot@ucsd.edu)